Sequestration and Removal of Multiple Small Molecule Contaminants using an Optimized Aptamer-Based Ultrafiltration System

Misael A. Romero-Reyes and Jennifer M. Heemstra*

Department of Chemistry, Emory University, Atlanta, GA 30322, United States

Abstract

Small-molecule toxins pose a significant threat to human health and the environment, and their removal is made challenging by their low molecular weight. Aptamers show promise as affinity reagents for binding these toxins, and recently aptamers have been utilized for both sensing and remediation applications. We have found that functionalization of ultrafiltration membranes with aptamers provides a convenient scaffold for toxin sequestration, but our initial efforts in this area were limited by low functionalization efficiencies and the ability to only capture a single target molecule. Herein, we describe detailed optimization of our aptamer-functionalized ultrafiltration membrane system and subsequent use for simultaneous removal of multiple small-molecule toxins. We examine multiple critical components involved in fabricating and functionalizing the membranes, including PEG polymer molecular weight for membrane fabrication, grafting conditions for pMAA attachment, and coupling reagents for aptamer functionalization. This screening enabled us to identify a set of unique conditions in which we were able to achieve high flux, near quantitative yield for DNA attachment, and effective overall depletion of both toxins and bacterial cells. Furthermore, we demonstrate attachment of multiple aptamers and subsequent parallel removal of atrazine, bisphenol A, and microcystin-LR in a complex lake water matrix. Our rigorous evaluation resulted in depletion of multiple small-molecule toxins and contaminants, demonstrating the potential of aptamer-functionalized membranes as point-of-use decontamination systems.

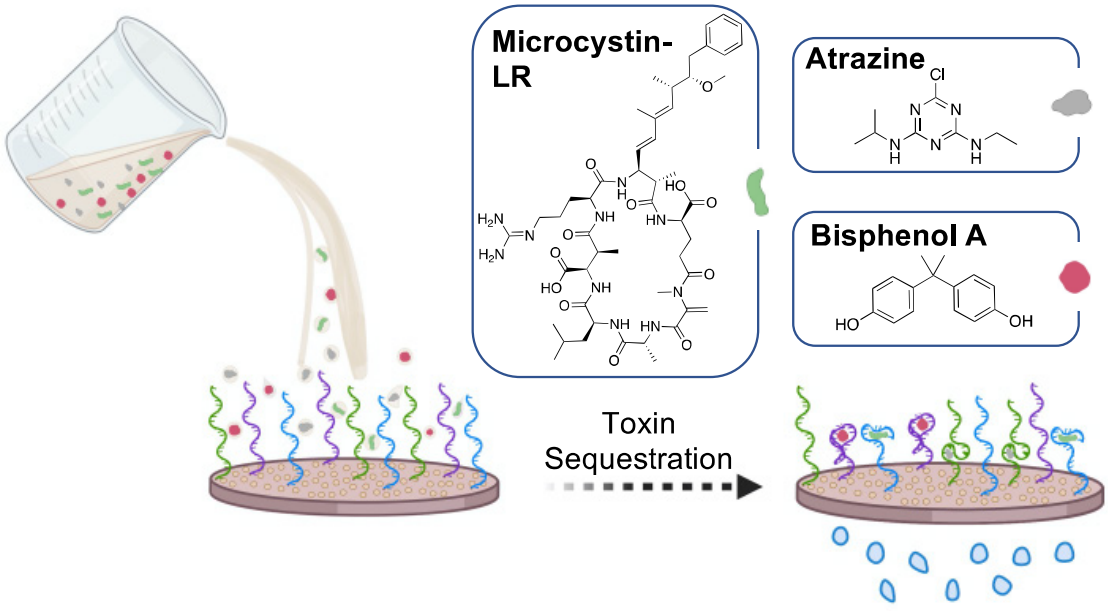

Introduction

Aptamers have emerged as promising affinity reagents for use in a wide range of applications,[1-3] owing to their ability to bind to a specific molecule of interest, their high chemical and thermal stability, and the ability to generate aptamers for a wide range of target molecules via *in vitro* selection.[4] To date, aptamers have been primarily used for biomedical applications including drug delivery, therapeutics, clinical diagnostics, imaging, and biomarker discovery.[5-6] However, more recently, they have also seen increasing use for environmental applications such as detection and removal of small-molecule toxins and contaminants in aqueous and biological matrices.[7-9]

A large number of aptamer-based biosensors have been reported for toxin detection and typically involve coupling of the target binding event to an electrochemical or optical output for quantification.[10-11] Given the ability of aptamers to bind to and sequester molecules of interest, researchers have also explored the use of aptamers in environmental water remediation, though examples of this use remain much more sparse in the literature.[12-13] To achieve sequestration, the aptamer must be immobilized on a solid support, and scaffolds that have been explored include TiO_2 and PLA-PEG nanoparticles, Sepharose beads, and hydrogels.[14-18] While effective, most of these methods require expensive machinery for fabrication or implementation and they can be susceptible to corrosion or biofouling. Additionally, most of these materials have not been shown to be capable of regeneration, limiting them to a single use.[12] Thus, while these technologies are able to remove the molecules of interest, they are limited by challenges with scale-up or time and material costs and are not amenable for point-of-use decontamination in resource limited environments.[19]

With an increase of contaminated water sources worldwide, the sequestration of small-molecule contaminants and toxins has become a priority and unique scaffolds are needed which can effectively sequester and remove these contaminants from an aqueous matrix.[20] Ultrafiltration membranes offer an advantageous scaffold, as they are fabricated from inexpensive materials using facile preparatory techniques and water can pass through them under pressures that can be easily generated using human power.[21] However, given their relatively large pore sizes, they lack the ability to sequester small molecules.[21] To overcome this challenge, we have previously demonstrated that aptamers can be covalently attached to ultrafiltration membranes by grafting poly(methacrylic acid) (pMAA) on the membrane, which introduces a carboxylic acid moiety, which can subsequently be reacted with an amine-modified aptamer.[22] We initially demonstrated the ability of this membrane system to remove Bisphenol A (BPA) from drinking water and environmental water samples. However, most water samples requiring purification contain multiple small-molecule contaminants including pharmaceuticals, pesticides, mycotoxins, and cyanotoxins, as well as small organisms such as bacteria.[23-24] To ensure practicality and efficacy in point-of-use applications, it is critical that an aptamer-based filtration device be able to retain and sequester multiple contaminants as well as small organisms.[25-26]

Herein, we systematically optimize each step of the process for fabrication of our aptamer functionalized membranes, from membrane formation to grafting to aptamer attachment. At each step, we rigorously characterize membrane performance or attachment yield to identify a set of optimized conditions. We also explore the relationship between membrane pore size and removal of bacteria (*Escherichia coli*), demonstrating the capacity to simultaneously sequester small molecules and single-celled organisms. Moreover, we establish the versatility of our membrane system by attaching a combination of different aptamers and demonstrating the ability to sequester multiple small molecules in parallel without impacting depletion efficacy. Together, this research advances the application of aptamer-functionalized membranes as a user-friendly and scalable approach to water purification.

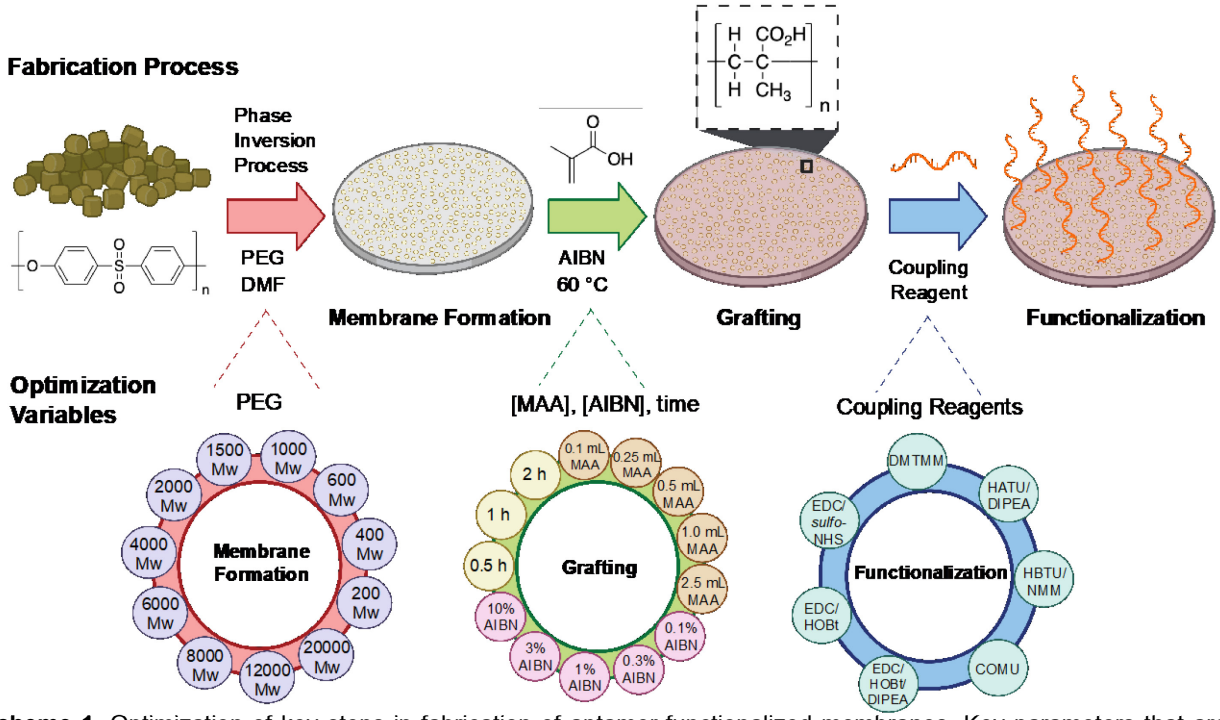

Scheme 1. Optimization of key steps in fabrication of aptamer-functionalized membranes. Key parameters that are explored include: (1) molecular weight of PEG additives used in membrane formation (2) concentrations of MAA and AIBN, and reaction time for pMAA grafting (3) coupling reagents used for aptamer functionalization.

Results and Discussion

For our initial demonstration of aptamer-functionalized membranes, we adapted standard conditions that had previously been reported in the literature for analogous fabrication and functionalization procedures.[22, 27-28] While this allowed for successful membrane generation, we recognized that significant benefit would be realized by systematically investigating and optimizing each step of the process. As outlined in **Scheme 1**, we explore a wide range of conditions for membrane formation, grafting, and functionalization, characterizing function at each step to arrive at an optimized protocol that maximizes both membrane flux and ability to remove small-molecule contaminants and small organisms.

Membrane Formation. Membranes are formed from PES using a phase inversion process, and PEG is used as an additive to promote pore formation.[29] Given that pore size impacts flux and other key characteristics, we reasoned that the molecular weight of the PEG was likely to play a substantial role in membrane performance. Thus, we started our optimization process by using PEG having different molecular weights, added to the dope solution when forming the ultrafiltration membranes. As shown in **Figure 1**, the use of different molecular weights of this additive changes the internal pore formation and the distribution of macrovoids, therefore modulating water filtration characteristics such as flux and solute rejection. We prioritized water flux, as maintaining high flux is critical to ensuring that the membranes can be operated in a point-of-use setting under human power (**Figure S1a-b**).[19] The data in **Figure 1a** demonstrate that there is an increase in flux as the PEG Mw increases from PEG200 until it reaches a plateau around PEG2000-PEG4000, before showing a steady decrease up to PEG20000, which was the

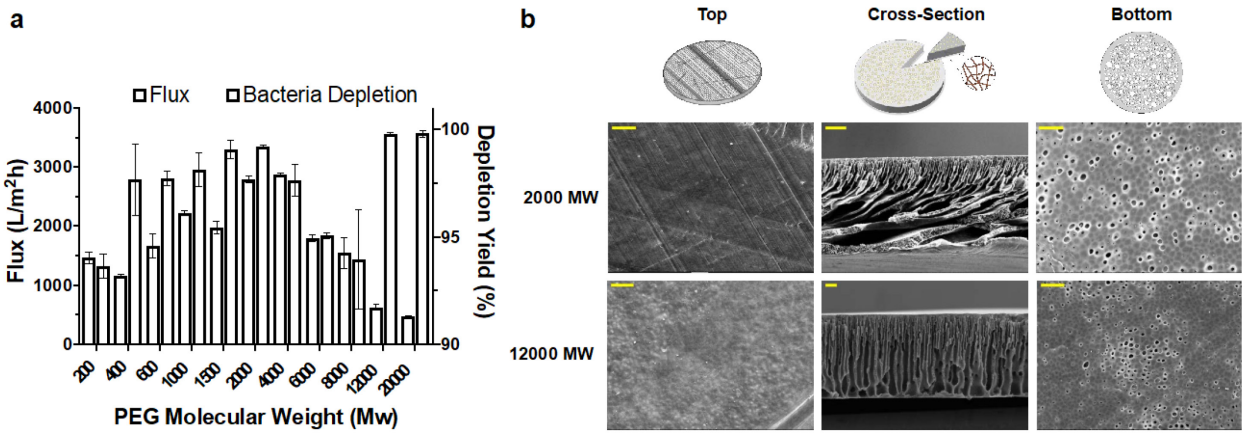

Figure 1. (a) Flux and bacteria depletion as a function of molecular weight of PEG dopant. The error bars represent standard deviation from 6 independent trials. **(b)** SEM images of membranes formed using PEG 2000 (top row) and PEG 12000 (bottom row), showing morphology at the top, bottom, and mid cross-section of the membrane. Scale bars are 10 μm for images of top and bottom of membrane and 50 μm for images of membrane cross-section.

largest PEG dopant tested. These data provided insight that membranes formed with PEG dopant in the range of PEG2000–PEG4000 provided optimal flux properties.

In considering the practical application of these water purification membranes, we recognized that most use would involve mixed matrices that contain both small-molecule contaminants and microorganisms such as bacteria.[30-31] We also recognized that since PEG molecular weight directly impacts pore size, this is the ideal metric to vary in order to optimize bacteria removal. Thus, we screened our membranes formed using various PEG sizes and quantified their ability to deplete *E. coli.* Water spiked with bacterial cells at a concentration of 8000 CFU/mL was filtered through each membrane and samples from before and after filtration were spread on agarose plates, incubated at 37 °C, and colonies quantified (**Figure S1c-e**). While the membranes having the lowest flux (PEG12000 and PEG20000) gave nearly quantitative bacterial depletion, we were surprised to observe that flux did not directly correlate with bacterial depletion as might be anticipated solely based on pore size (**Figure 1a**).

Considering both flux and bacterial removal, we concluded that PEG2000 serves as the best dopant size for preparing our ultrafiltration membranes. However, due to the exceptionally high performance with bacterial depletion and the recognition that other smaller microorganisms may also be present in water samples, we also chose to continue investigating membranes formed using PEG12000, as some sacrifice of flux could be a favorable tradeoff for higher bacterial depletion. Membranes formed using each of these PEG dopant sizes were characterized using SEM (**Figure 1b**). The PEG2000 membranes displayed prominent large macrovoids in the cross-section, which was also consistent with the formation of more pores on the bottom of the membrane, and therefore higher flux. In contrast, the PEG12000 membranes show fewer pores, which likely explains the lower flux and higher bacterial depletion.

Membrane Grafting. The next step in our membrane fabrication process is grafting of the PES with pMAA via radical polymerization. The carboxylic acid functional groups on pMAA serve two important purposes, in that they increase the hydrophilicity of the membrane for better use with aqueous matrices[32-33] and provide an attachment point for subsequent functionalization with amine-modified aptamers. Given that maximizing aptamer attachment represents a key desired outcome, we analyzed grafting conditions by monitoring DNA functionalization yield using a

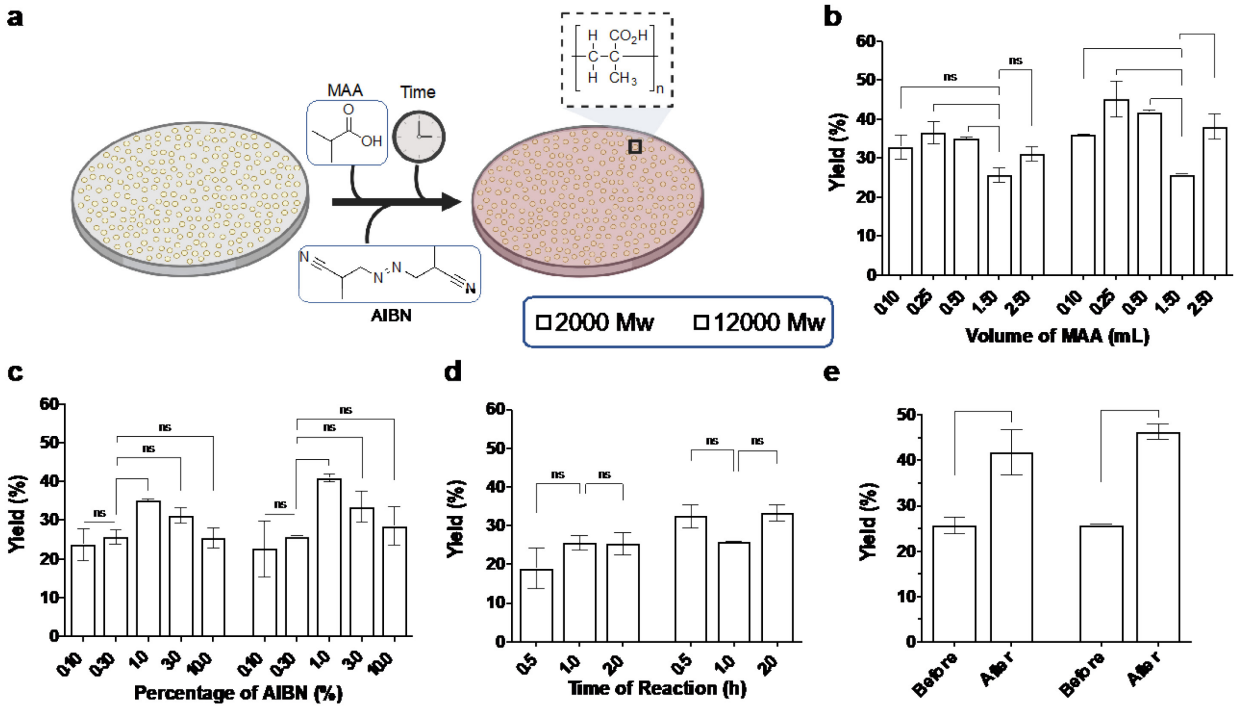

Figure 2. (a) Optimization of membrane grafting using membranes formed with PEG2000 and PEG12000. Yield of aptamer attachment resulting from: **(b)** varying volumes of MAA (added to 5 mL water); **(c)** varying concentrations of AIBN initiator; **(d)** varying polymerization reaction time. **(e)** Incorporating all of the optimized conditions results in a significant increase in yield for aptamer attachment. The error bars represent standard deviation of 3 independent trials (*p < 0.05, **p < 0.01, one-way ANOVA with Tukey's multiple comparison for **(b) – (d)** and two-tailed t-test for **(e)**).

constant set of coupling conditions. Our membrane has a surface area of 5.51 cm^2 and 100% yield would represent 5.45 $nmol/cm^2$, given that the maximum amount of aptamer used per reaction is 30 nmol. To optimize grafting, we surveyed a range of methacrylic acid (MAA) volumes (added to 5 mL water for each reaction), 2,2′-azobis(2-methylpropionitrile) AIBN concentrations, and polymerization reaction times with our two previously identified PEG2000 and PEG12000 membranes (**Figure 2**). We benchmarked the performance of each membrane against our previously reported conditions (1.5 mL of MAA, 0.3% AIBN, and 1 h of reaction time after MAA addition). We then reacted each membrane with the anti-BPA aptamer[34] using *N*-(3-dimethylaminopropyl)-*N′*-ethylcarbodiimide hydrochloride/*N*-hydroxysulfosuccinimide sodium salt (EDC/*sulfo*-NHS) as a coupling reagent and quantified aptamer attachment efficiency as previously reported.[22] In short, yield was determined by quantifying the change in concentration of the fluorophore labeled aptamer in the supernatant before and after reaction when exposed to the grafted membrane and using the appropriate coupling reagent in MOPS buffer.

For MAA volume, we observe reproducible impacts on aptamer functionalization, but no distinct relationship between the two variables for either of the membranes (**Figure 2b**). Given that the best performance was obtained using 0.25 mL of MAA, we identified this as our volume for use in future experiments. We do note that this condition provides significantly higher attachment compared to the 1.5 mL of MAA used in our initial experiments. In the case of AIBN concentration, we observe that lower amounts of AIBN than used our previously described conditions (0.3%) does not produce a significant difference in functionalization yield. However, we do note a significant functionalization yield increase when AIBN concentration is increased from 0.3% to 1%, but further increases to 3% and 10% have an opposite effect (**Figure 2c**). One potential

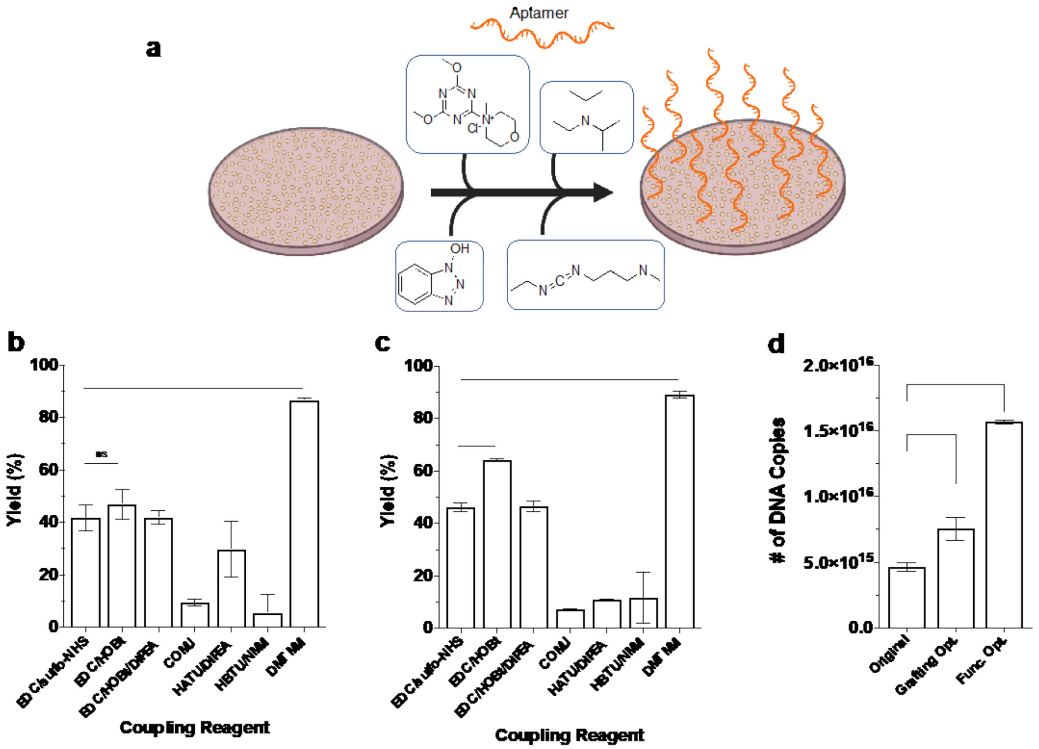

Figure 3. (a) Optimization of aptamer functionalization using various coupling reagents. Each coupling condition was tested on membranes generated with **(b)** PEG2000 and **(c)** PEG12000. **(d)** Significant increase in DNA copy number after completion of the comprehensive grafting and functionalization optimization. The error bars represent standard deviation of 3 independent trials (*p < 0.05, **p < 0.01, ***p < 0.001, two-tailed t-test).

explanation for these results could be linked to the size of pMAA polymers formed. We hypothesize that increased AIBN should lead to higher numbers of initiation events, and while this could give higher MAA loading, it could also decrease the average pMAA molecular weight if all of the MAA is consumed. While we did not directly study this factor, the size of pMAA may impact functionalization yield, as longer chains will provide greater relief from the steric constraints of the membrane itself. Independent of reasoning for the optimized concentration, we identified 1% AIBN as the optimal condition. As a final parameter, we decided to also vary polymerization reaction time. We varied the reaction time from 0.5-2 h, but no significant differences were observed when increasing or lowering the time, so we decided to maintain our original polymerization time of 1 h (**Figure 2d**).

After individually optimizing each reaction parameter, we compared the optimized conditions to those in our previous report, and found that our newly proposed grafting conditions increase the yield for aptamer attachment by ~20% for each membrane (**Figure 2e**). These new conditions also showed an increase in functionalization yield with aptamers for other small-molecule targets such as atrazine[35], acetamiprid[36-37], and Microcystin-LR (MC-LR)[38] (**Figure S2**). Thus, our approach is adaptable to aptamers (or other nucleic acids) having varying lengths and secondary structures.

Membrane Functionalization. The DNA aptamer represents the costliest component of the membrane system, and thus optimizing yield for attachment is a critical goal for improving the practicality of scaleup. We were encouraged by the increased yield we were able to obtain through modification of our grafting conditions, and hypothesized that further gains might be realized by

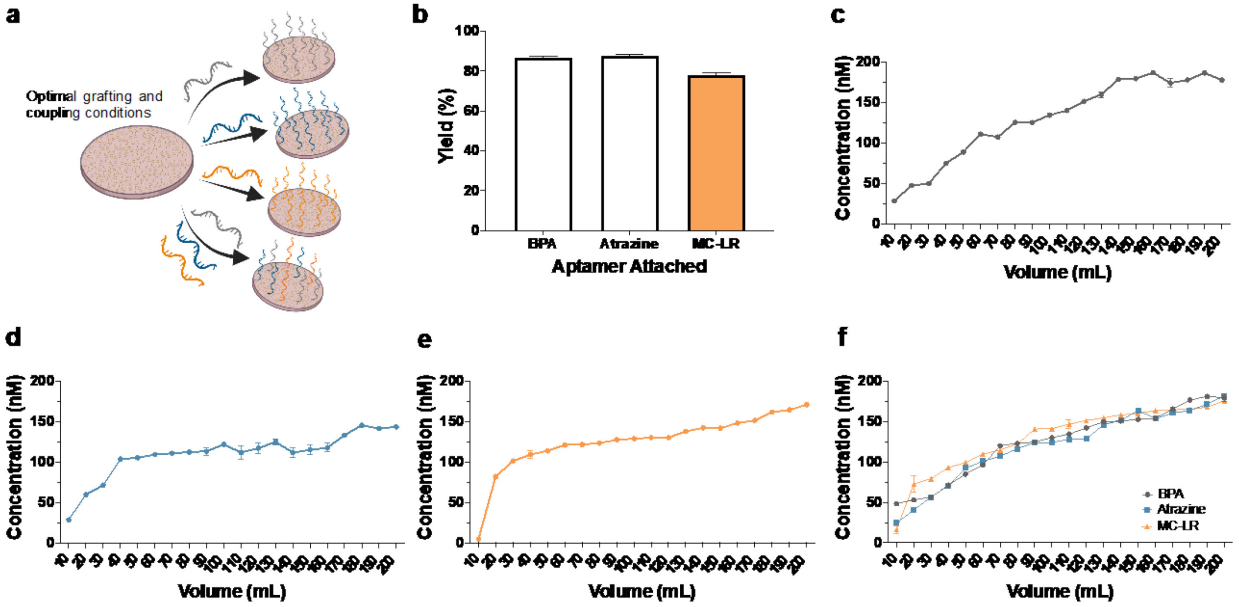

Figure 4. (a) Membrane functionalization with aptamers for BPA (gray), Atrazine (blue), and Microcystin-LR (orange). **(b)** Functionalization efficacy for each aptamer. Error bars represent standard deviation of 3 independent trials. Depletion capacity of membranes functionalized with aptamer for **(c)** BPA only, **(d)** Atrazine only, and **(e)** MC-LR only, using 200 nM spiked Milli-Q water as the feed solution. **(f)** Simultaneous depletion of BPA, atrazine, and MC-LR from a membrane functionalized with all three aptamers. Error bars for depletion represent standard deviation of 2 independent trials.

also screening reaction conditions for the bioconjugation reaction itself. We tested a variety of common coupling reagents used for amide bond formation[39] and compared these to our previously reported protocol using EDC/*sulfo*-NHS (**Figure 3b-c**). We observed that the addition of different catalysts to the EDC such as 1-hydroxybenzotriazole (HOBt) and *N,N*-diisopropylethylamine (DIPEA) had little effect on yield, with only a small increase observed using HOBt with the PEG12000 membrane. Other coupling reagents such as (1-cyano-2-ethoxy-2-oxoethylidenaminooxy)dimethylamino-morpholino-carbenium hexafluorophosphate (COMU), 1-[*bis*(dimethylamino)methylene]-1*H*-1,2,3-triazolo[4,5-b]pyridinium 3-oxid hexafluorophosphate (HATU) and N,N,N′,N′-tetramethyl-O-(1*H*-benzotriazol-1-yl)uronium hexafluorophosphate (HBTU) show a decrease in yield for both membranes. However, we were very encouraged to observe that 4-(4,6-dimethoxy-1 ,3,5-triazin-2-yl)-4-methylmorpholinium chloride (DMTMM), showed outstanding results, with an 87-90% functionalization yield across both membranes. **Figure 3d** demonstrates the combined effects of our optimization study, as we are able to more than triple the amount of DNA attached to the membrane. Importantly, with the high yields obtained in our final conditions, very little DNA is wasted in the fabrication process. Moreover, we hypothesize that higher functionalization densities could be obtained by using increased amounts of DNA.

Multi-Analyte Removal. After identifying our optimized conditions for membrane formation (PEG2000 or PEG12000 dopant), membrane grafting (0.25 mL MAA, 1% AIBN, 1 h reaction time), and functionalization (DMTMM), we sought to demonstrate the versatility of the membrane system to be used for depletion of structurally-diverse small-molecule contaminants, or even simultaneous removal of multiple contaminants. First, we created single-aptamer membranes using the aptamers for BPA, atrazine, and MC-LR, which represent a wide range of nucleic acid sizes. Encouragingly, we observed consistent high yields for attachment of each of these aptamers: 87% for BPA (14 nt), 88% for atrazine (32 nt), and 79% for MC-LR (60 nt) (**Figure 4a-**

b). As a control, we subjected an ungrafted membrane to the same coupling conditions and observed no attachment (**Figure S3**).

To test depletion efficiency and selectivity for each small-molecule target, water spiked with 200 nM of contaminant was flowed through each membrane, and concentration of each small-molecule in the eluent was quantified by HPLC. As expected, we observed higher depletion for the early fractions, as more aptamer is available for binding, and this is consistent with our earlier report. We were unsure, however, whether all of the aptamers would be capable of depletion with the same efficiency. Thus, we were pleased to observe similar depletion curves for each of the single-aptamer membranes (**Figure 4c-e)**. We also found that total ligand binding capacities were similar at 14 nmol for BPA, 18 nmol for atrazine, and 15 nmol for MC-LR.

After demonstrating successful depletion of each contaminant on a single-aptamer membrane, we focused on exploring whether we could attach all three different aptamers to a single membrane without compromising functionalization yield or depletion capacity. We observed similar functionalization yields as had been achieved for single-aptamer membranes (**Figure S5**), which is especially encouraging as it demonstrates that our overall loading of DNA on the membrane can be increased far beyond the levels used in our initial experiments. We then subjected the membrane to filtration with water spiked with 200 nM of each of the three contaminants, and observed that the depletion capacity of the tri-aptamer membrane was similar to that of each of the single-aptamer membranes, demonstrating that increased DNA loading and the presence of multiple aptamers and targets does not significantly impact performance (**Figure 4f, Figure S6**).

Most importantly, comparing the depletion capacities from our previous study with those of our optimized system revealed a 5-fold increase in capacity for membranes of the same size, which is largely attributable to our increased yield for functionalization. This is important, as increasing capacity allows a membrane to filter a greater volume of water before breaking through the allowable limits for each toxin in drinking water. While this initial demonstration is performed using a relatively small volume of water, the membranes used in practical applications would be significantly larger and thus have higher removal capacity. For example, the dimensions of a typical personal-use water purification membrane are 23 cm x 23 cm, which is 34-fold larger than the membranes used in our study, and thus would enable the purification of ~7 L of water

Application in Environmental Samples. To demonstrate the practical utility of aptamer-functionalized membranes in environmental samples, we tested our system in lake water from a local source. We obtained lake water from Chandler Lake-Lullwater Preserve at Emory University and evaluated the presence of the contaminants that we were interested in removing. After finding that these contaminants were not present at detectable levels in this water source, we generated a contrived environmental sample by spiking the water with the same concentration of contaminants used in our previous experiments (**Figure S7**). As a control, we filtered this sample through a grafted membrane with no aptamers attached, and we observed that the concentration of the different contaminants remains constant, demonstrating that depletion does not arise from

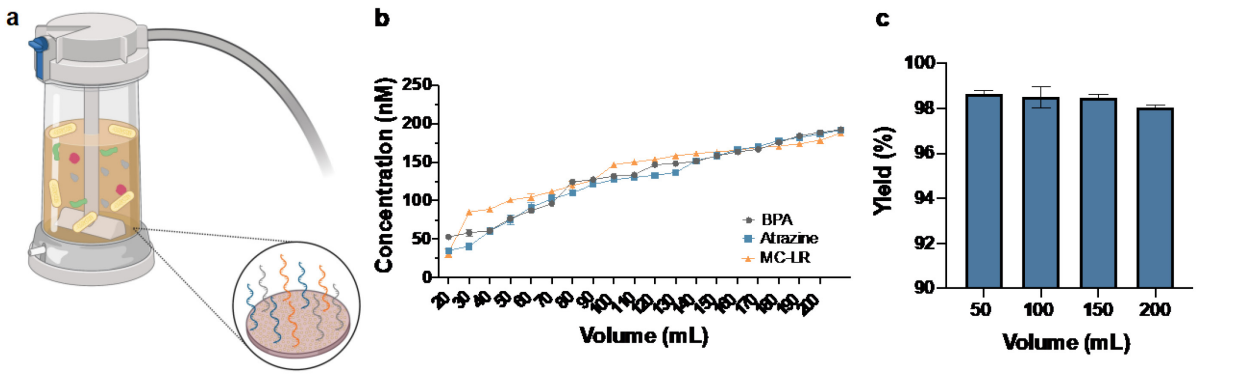

Figure 5. (a) Depletion of small-molecule contaminants using a lake water sample containing spiked contaminants and bacteria. **(b)** Depletion capacity of different contaminants using a membrane functionalized with multiple aptamers. **(c)** Bacteria depletion yield as a function of volume of filtered sample. Error bars represent standard deviation of 2 independent trials.

non-specific adsorption of the small molecules (**Figure S7a**). We then repeated the filtration using a tri-functionalized membrane having BPA, atrazine, and MC-LR aptamers, and these samples showed depletion of their respective small molecules in a similar manner to that observed for a tap water sample (**Figure S7b** and **Tables S2-S4**). This further demonstrates the versatility and utility of the purification system we have created, as it is able to simultaneously remove multiple small-molecule toxins from a complex environmental sample. Finally, we explored filtration of a sample of lake water containing all three small-molecule contaminants as well as microorganisms (*E. coli*). The small molecule contaminants and bacteria were spiked into the sample as described above. We then filtered the sample using a tri-aptamer functionalized membrane, and analysis of the resulting filtrate showed similar levels of depletion as observed in tap water samples and for individual depletion of small molecules and bacterial cells (**Figure 5**). We were able to remove 13.5 nmol of BPA, 14.5 nmol of atrazine, and 13.5 nmol of microcystin-LR. Most importantly, our system was able to remove 98.5% of bacteria and function as expected despite the complex matrix of a lake water sample

Conclusions

In summary, we describe here the optimization of membrane fabrication, grafting, and aptamer functionalization to maximize aptamer loading and thus toxin depletion of ultrafiltration membranes. We observed that PEG2000 is an ideal pore forming agent in membrane formation as it provides membranes having high flux and the ability to remove most bacterial cells. Our grafting conditions screen showed that increasing the concentration of the radical initiator and decreasing the concentration of MAA relative to our previous conditions provided improved aptamer attachment yields. We were also able to identify a high-yielding coupling reagent (DMTMM) that aids in the amide bond formation reaction to give near quantitative DNA functionalization. With these enhanced parameters, we were able to reliably attach aptamers having varying sizes and secondary structures and achieve depletion of structurally diverse contaminants. Furthermore, we were able to attach three aptamers to the membrane, overall tripling the DNA loading and enabling simultaneous removal of three contaminants without a significant decrease in depletion efficiency.

Given the reported improvements in functionalization yield, we hypothesize that the membranes could be scaled to create personal use filters able to purify the equivalent amount of drinking water for one person for one day. And, we have reported previously that the membrane can be easily regenerated using a small volume of warm water to reversibly denature the aptamers.[22]

Additionally, the flexibility to work with multiple aptamer-analyte systems will allow for the creation of membranes that are customized to local water purification needs. Together, aptamer-functionalized ultrafiltration membranes hold significant promise for point-of-use decontamination of water, offering potential to advance environmental and human health.

Experimental Section

Materials: Chemicals including the polymers, coupling reagents, molecular contaminants were obtained from Sigma Aldrich Corporation (St. Louis, MO, USA) and were used without further purification. Chemicals include poly(oxy-1,4-phenylenesulfonyl-1,4-phenylene) (PES), methacrylic acid (MAA), poly(ethylene glycol)- various molecular weights (PEG), 2,2′-azobis(2-methylpropionitrile) (AIBN), *N,N*-dimethylformamide (DMF), *N*-(3-dimethylaminopropyl)-*N′*-ethylcarbodiimide hydrochloride (EDC), *N*-hydroxysulfosuccinimide sodium salt (*sulfo*-NHS), (1-cyano-2-ethoxy-2-oxoethylidenaminooxy)dimethylamino-morpholino-carbenium hexafluorophosphate (COMU), 1-[*bis*(dimethylamino)methylene]-1*H*-1,2,3-triazolo[4,5-b]pyridinium 3-oxidhexafluorophosphate (HATU), 3-hydroxytriazolo[4,5-b]pyridine (HOAt), 1-hydroxybenzotriazole (HOBt), *N,N*-diisopropylethylamine (DIPEA), N,N,N′,N′-tetramethyl-O-(1H-benzotriazol-1-yl)uronium hexafluorophosphate (HBTU), 4-methylmorpholine (NMM), 4-(4,6-dimethoxy-1,3,5-triazin-2-yl)-4-methylmorpholinium chloride (DMT-MM), bisphenol A (BPA), mMicrocystin-LR (MC-LR), and atrazine. DNA sequences (**Table S1-S2**) were custom-synthesized from University of Utah DNA/Peptide Synthesis Core (Salt Lake City, UT, USA) and from Integrated DNA Technologies (Coralville, IA, USA). The purity and length of aptamer sequences was validated using denaturing PAGE. Membranes were crafted using a Elcometer® 3580/4 casting knife film applicator. Membrane flux experiments were accomplished using an Amicon® Stirred Cell 50 mL (UFSC05001) from Millipore-Sigma (Burlington, MA, USA). Colonies were counted using a colony counter pen manufactured by VWR® (Radnor, PA, USA).

Fabrication of ultrafiltration membranes. In a closed glass container, PES pellets (2.0 g, 15% w/w), PEG (1.28 g, 10% w/w), and DMF (10 mL, 75% w/w) were mixed at room temperature. This solution was agitated using a nutating mixer until full homogenization was achieved. This dope solution was divided into two equivalent portions and each portion was spread on a 20 cm x 20 cm glass plate using a casting knife film applicator at a width of 500 µm. The glass was then submerged in a tub containing deionized water, causing precipitation of the film and thus formation of the membrane. The membrane remained in the water bath until it detached from the glass. The rough edges were excised, and the membrane was washed with copious amounts of water for 12 h to remove any non-precipitated content. Circular membranes were produced using a stainless-steel round cutter with a size of 1.75 in, followed by trimming of the excess membrane with scissors.

Grafting of ultrafiltration membranes. The circular membrane was combined with 20 mL of degassed water (using N_2) in an appropriate glass vessel. Radicals were formed by the addition of differing amounts of AIBN under a N_2 atmosphere at a temperature of 60 °C. The membrane and initiator were reacted for 20 min on a nutating mixer at 500 rpm. MAA (various amounts) was added dropwise to the reaction mixture to prevent self-polymerization. The reaction mixture was diluted with 5 mL of degassed water and reacted for 1 h at 60 °C. The membrane was removed from the reaction mixture and stored in 50 mL of fresh water. Unbound pMAA was removed by washing with NaOH (1 N, 3 x 50 mL) and water (3 x 50 mL) for 7 min each. The washes followed the alternating sequence: NaOH → H_2O → NaOH → H_2O → NaOH → H_2O. Grafting yield was determined by functionalizing a fluorophore labeled antisense-BPA aptamer (10 µM) using the initial coupling conditions (EDC/*sulfo*-NHS), to verify how much aptamer was attached to the grafted membrane.

Functionalizing grafted membranes. The circular membranes (with optimized grafted conditions) were activated with different coupling reagents with concentrations ranging from 60 – 300 mM for 20 min. (10 min on each side of the membrane). FAM-labeled or Cy3-labeled amine-modified DNA (10 μM) was prepared for membrane functionalization and attachment quantification by diluting the DNA in MOPS buffer (1 M, 0.5 N NaCl, pH 8.5). For initial characterization, a small (50 μL) aliquot was removed from the solution. To ensure thorough functionalization, the membrane was added to the DNA solution and shaken in the nutating mixer for 24 h. The membranes were washed with MOPS buffer (3 x 10 mL) and water (3 x 10 mL) to remove any unbound DNA and further stored in fresh water until further usage. Yield was determined by the change in concentration of the fluorophore labeled aptamer in the supernatant before and after reaction. DNA copy number was estimated from the nanomoles of aptamer that were conjugated to the membrane.

Scanning Electron Microscopy. Circular ultrafiltration membranes were cut into 0.5 x 0.5 cm squares and coated with 20 nm of AuPd in a Denton Desktop II sputter coater. Cross-sections were obtained by submerging the membrane in liquid nitrogen for 1 min and then tearing using tweezers to obtain a clean cross-section cut. SEM (Topcon Ds 130f in high vacuum mode) was used to visualize different morphological features of the membrane samples. Images were analyzed using ImageJ.

Flux experiments. The membranes were compressed using the stirred-cell filtration apparatus for 10 min at a pressure of 2.5 bar with N_2. Readings were measured at 1 bar. The time required for the water volume to decrease from V_1= 40 mL to V_2= 20 mL (ΔV= 20 mL) was measured. Flux (J) was calculated as shown below in Equation 1 and reported as L/m^{2}h. Q_p is the permeate flow (L/h) and A_{system} is the surface area of the membrane in m^2.

Equation 1: Calculation of flux.

$$J = \frac{Q_p}{A_{system}}$$

Bacterial depletion. Overnight cultures of *Escherichia coli (E. coli)* were started in Luria-Bertani (LB) broth and grown at 37 ºC shaking at 200 RPM. Exponential phase cultures (OD_{600} = 0.3 - 0.6) were then used to create solutions of 8000 cells/mL in water. Water (50 mL) spiked with bacteria was filtered through an ultrafiltration membrane using the stirred-cell filtration apparatus. Aliquots of solution, taken before and after filtration, were diluted 10- and 100-fold and were streaked in separate agar plates (100 μL) and were incubated overnight at 37 ºC. Colonies were counted by hand using a colony counter pen to assess the number of colonies formed before and after filtration to determine the percentage of bacteria depletion.

Small-molecule depletion. Depletion of small-molecule contaminants using the functionalized membrane was investigated by filtering a spiked water sample (200 nM of BPA, MC-LR, atrazine, or all three) as the feed solution. This was performed using a stirred cell apparatus by compressing the membranes for 10 min at a pressure of 2.5 bar with N_2. The system was filtered at 1 bar and the permeate (10 mL fractions) was collected and 1.5 mL of each fraction was concentrated using vacuum centrifugation. The samples were analyzed as previously described.[22] In short, using HPLC, a calibration curve ranging from 0 nM-200 nM was obtained and concentrations of the different fractions were determined by comparing peak area to that from a calibration curve.

Associated Content

Supporting Information.

The Supporting Information is available free of charge at http://pubs.acs.org.

DNA sequences, flux and bacteria protocols, and control data for membrane formation, grafting, functionalization, and small-molecule depletion.

Author Information

Corresponding Author

Jennifer M. Heemstra- *Department of Chemistry, Emory University, Atlanta, Georgia 30322, United States;* ocrid.org/0000-0002-7691-8526, jen.heemstra@emory.edu

Authors

Misael Romero-Reyes- *Department of Chemistry, Emory University, Atlanta, Georgia 30322, United States;* ocrid.org/0000-0003-4614-4512

Author Contributions

The manuscript was written through contributions of all authors. All authors have given approval to the final version of the manuscript.

Funding

This work was supported by the National Science Foundation (CBET 1818476 to J.M.H.).

Notes

The authors declare no competing financial interest.

Acknowledgements

The authors would like to thank Arthur McCanna from the Robert P. Apkarian Integrated Electron Microscopy Core (IEMC) at Emory University for providing training and insight during SEM experiments.

References

1. Liu, L. S.; Wang, F.; Ge, Y.; Lo, P. K., Recent Developments in Aptasensors for Diagnostic Applications. *ACS Applied Materials & Interfaces* **2021,** *13* (8), 9329-9358.
2. Ni, S.; Zhuo, Z.; Pan, Y.; Yu, Y.; Li, F.; Liu, J.; Wang, L.; Wu, X.; Li, D.; Wan, Y.; Zhang, L.; Yang, Z.; Zhang, B.-T.; Lu, A.; Zhang, G., Recent Progress in Aptamer Discoveries and Modifications for Therapeutic Applications. *ACS Applied Materials & Interfaces* **2021,** *13* (8), 9500-9519.
3. Fan, C.; Wang, S.; Schanze, K.; Fernandez, L. E., Materials Applications of Aptamers. *ACS Applied Materials & Interfaces* **2021,** *13* (8), 9289-9290.
4. Ruscito, A.; DeRosa, M. C., Small-Molecule Binding Aptamers: Selection Strategies, Characterization, and Applications. *Frontiers in Chemistry* **2016,** *4* (14).
5. Afrasiabi, S.; Pourhajibagher, M.; Raoofian, R.; Tabarzad, M.; Bahador, A., Therapeutic applications of nucleic acid aptamers in microbial infections. *Journal of Biomedical Science* **2020,** *27* (1), 6.
6. Xie, S.; Ai, L.; Cui, C.; Fu, T.; Cheng, X.; Qu, F.; Tan, W., Functional Aptamer-Embedded Nanomaterials for Diagnostics and Therapeutics. *ACS Applied Materials & Interfaces* **2021,** *13* (8), 9542-9560.
7. Saad, M.; Faucher, S. P., Aptamers and Aptamer-Coupled Biosensors to Detect Water-Borne Pathogens. *Frontiers in Microbiology* **2021,** *12* (304).
8. Schmitz, F. R. W.; Valério, A.; de Oliveira, D.; Hotza, D., An overview and future prospects on aptamers for food safety. *Applied Microbiology and Biotechnology* **2020,** *104* (16), 6929-6939.
9. McConnell, E. M.; Nguyen, J.; Li, Y., Aptamer-Based Biosensors for Environmental Monitoring. *Frontiers in Chemistry* **2020,** *8* (434).
10. Arvand, M.; Mirroshandel, A. A., An efficient fluorescence resonance energy transfer system from quantum dots to graphene oxide nano sheets: Application in a photoluminescence aptasensing probe for the sensitive detection of diazinon. *Food Chemistry* **2019,** *280*, 115-122.
11. Wei, X.; Zhou, W.; Sanjay, S. T.; Zhang, J.; Jin, Q.; Xu, F.; Dominguez, D. C.; Li, X., Multiplexed Instrument-Free Bar-Chart SpinChip Integrated with Nanoparticle-Mediated Magnetic Aptasensors for Visual Quantitative Detection of Multiple Pathogens. *Analytical Chemistry* **2018,** *90* (16), 9888-9896.
12. Bilibana, M. P.; Citartan, M.; Yeoh, T. S.; Rozhdestvensky, T. S.; Tang, T.-H., Aptamers as the Agent in Decontamination Assays (Apta-Decontamination Assays): From the Environment to the Potential Application In Vivo. *J Nucleic Acids* **2017,** *2017*, 3712070-3712070.
13. Schax, E.; Lönne, M.; Scheper, T.; Belkin, S.; Walter, J.-G., Aptamer-based depletion of small molecular contaminants: A case study using ochratoxin A. *Biotechnology and Bioprocess Engineering* **2015,** *20* (6), 1016-1025.
14. Chen, B.; Ye, Q.; Zhou, K.; Wang, Y., Adsorption and separation of HCV particles by novel affinity aptamer-functionalized adsorbents. *Journal of Chromatography B* **2016,** *1017-1018*, 174-181.
15. Hu, X.; Tulsieram, K. L.; Zhou, Q.; Mu, L.; Wen, J., Polymeric nanoparticle–aptamer bioconjugates can diminish the toxicity of mercury in vivo. *Toxicology Letters* **2012,** *208* (1), 69-74.
16. Song, M. Y.; Jurng, J.; Park, Y.-K.; Kim, B. C., An aptamer cocktail-functionalized photocatalyst with enhanced antibacterial efficiency towards target bacteria. *Journal of Hazardous Materials* **2016,** *318*, 247-254.
17. Hu, X.; Mu, L.; Zhou, Q.; Wen, J.; Pawliszyn, J., ssDNA Aptamer-Based Column for Simultaneous Removal of Nanogram Per Liter Level of Illicit and Analgesic Pharmaceuticals in Drinking Water. *Environmental Science & Technology* **2011,** *45* (11), 4890-4895.

18. Wang, J.; Shen, H.; Hu, X.; Li, Y.; Li, Z.; Xu, J.; Song, X.; Zeng, H.; Yuan, Q., A Targeted "Capture" and "Removal" Scavenger toward Multiple Pollutants for Water Remediation based on Molecular Recognition. *Adv Sci (Weinh)* **2016,** *3* (3), 1500289.
19. Pooi, C. K.; Ng, H. Y., Review of low-cost point-of-use water treatment systems for developing communities. *npj Clean Water* **2018,** *1* (1), 11.
20. Obotey Ezugbe, E.; Rathilal, S., Membrane Technologies in Wastewater Treatment: A Review. *Membranes (Basel)* **2020,** *10* (5), 89.
21. Lee, A.; Elam, J. W.; Darling, S. B., Membrane materials for water purification: design, development, and application. *Environmental Science: Water Research & Technology* **2016,** *2* (1), 17-42.
22. Romero-Reyes, M. A.; Heemstra, J. M., Small-Molecule Sequestration Using Aptamer-Functionalized Membranes. *ACS Materials Letters* **2019,** *1* (5), 568-572.
23. Rojas, S.; Horcajada, P., Metal–Organic Frameworks for the Removal of Emerging Organic Contaminants in Water. *Chemical Reviews* **2020,** *120* (16), 8378-8415.
24. Rathi, B. S.; Kumar, P. S., Application of adsorption process for effective removal of emerging contaminants from water and wastewater. *Environmental Pollution* **2021,** *280*, 116995.
25. Brown, K. W.; Gessesse, B.; Butler, L. J.; MacIntosh, D. L., Potential Effectiveness of Point-of-Use Filtration to Address Risks to Drinking Water in the United States. *Environmental Health Insights* **2017,** *11*, 1178630217746997.
26. Yoo, H.; Jo, H.; Oh, S. S., Detection and beyond: challenges and advances in aptamer-based biosensors. *Materials Advances* **2020,** *1* (8), 2663-2687.
27. Li, Y.; Gabriele, E.; Samain, F.; Favalli, N.; Sladojevich, F.; Scheuermann, J.; Neri, D., Optimized Reaction Conditions for Amide Bond Formation in DNA-Encoded Combinatorial Libraries. *ACS Combinatorial Science* **2016,** *18* (8), 438-443.
28. Shi, Q.; Su, Y.; Ning, X.; Chen, W.; Peng, J.; Jiang, Z., Graft polymerization of methacrylic acid onto polyethersulfone for potential pH-responsive membrane materials. *Journal of Membrane Science* **2010,** *347* (1), 62-68.
29. Ma, Y.; Shi, F.; Ma, J.; Wu, M.; Zhang, J.; Gao, C., Effect of PEG additive on the morphology and performance of polysulfone ultrafiltration membranes. *Desalination* **2011,** *272* (1), 51-58.
30. Xu, H.; Guo, L., Molecular size-dependent abundance and composition of dissolved organic matter in river, lake and sea waters. *Water Research* **2017,** *117*, 115-126.
31. Zhang, H.; Wang, Y.; Chen, S.; Zhao, Z.; Feng, J.; Zhang, Z.; Lu, K.; Jia, J., Water Bacterial and Fungal Community Compositions Associated with Urban Lakes, Xi'an, China. *International Journal of Environmental Research and Public Health* **2018,** *15* (3).
32. Yang, B.; Yang, X.; Liu, B.; Chen, Z.; Chen, C.; Liang, S.; Chu, L.-Y.; Crittenden, J., PVDF blended PVDF-g-PMAA pH-responsive membrane: Effect of additives and solvents on membrane properties and performance. *Journal of Membrane Science* **2017,** *541*, 558-566.
33. Zheng, C.; Zhou, Y.; Zhang, H., Facile Preparation of Well-Defined Uniform Hydrophilic Hairy Hollow Functional Polymer Micro- and Nanoparticles. *ACS Applied Polymer Materials* **2020,** *2* (2), 220-233.
34. Lee, E.-H.; Lim, H. J.; Lee, S.-D.; Son, A., Highly Sensitive Detection of Bisphenol A by NanoAptamer Assay with Truncated Aptamer. *ACS Applied Materials & Interfaces* **2017,** *9* (17), 14889-14898.
35. Williams, R. M.; Crihfield, C. L.; Gattu, S.; Holland, L. A.; Sooter, L. J., In Vitro Selection of a Single-Stranded DNA Molecular Recognition Element against Atrazine. *International Journal of Molecular Sciences* **2014,** *15* (8), 14332-14347.
36. Shi, H.; Zhao, G.; Liu, M.; Fan, L.; Cao, T., Aptamer-based colorimetric sensing of acetamiprid in soil samples: Sensitivity, selectivity and mechanism. *Journal of Hazardous Materials* **2013,** *260*, 754-761.

37. He, J.; Liu, Y.; Fan, M.; Liu, X., Isolation and Identification of the DNA Aptamer Target to Acetamiprid. *Journal of Agricultural and Food Chemistry* **2011,** *59* (5), 1582-1586.
38. Ng, A.; Chinnappan, R.; Eissa, S.; Liu, H.; Tlili, C.; Zourob, M., Selection, Characterization, and Biosensing Application of High Affinity Congener-Specific Microcystin-Targeting Aptamers. *Environmental Science & Technology* **2012,** *46* (19), 10697-10703.
39. Valeur, E.; Bradley, M., Amide bond formation: beyond the myth of coupling reagents. *Chemical Society Reviews* **2009,** *38* (2), 606-631.